Proc IMechE Part D: J Automobile Engineering 2017, Vol. 231(3) 360–371

ON THE RELATION BETWEEN EXTERNAL STRUCTURE AND INTERNAL CHARACTERISTICS IN THE NEAR-NOZZLE FIELD OF DIESEL SPRAYS.

J. Benajes, F. J. Salvador (*), M. Carreres, D. Jaramillo.

CMT-Motores Térmicos. Universitat Politècnica de València, Spain

Camino de Vera s/n, E-46022 Spain.

(*) Corresponding author:

Dr. F. Javier Salvador, fsalvado@mot.upv.es

CMT-Motores Térmicos, Universitat Politècnica de València

Camino de Vera s/n, E-46022 Spain.

Telephone: +34-963879659

FAX: +34-963877659

ABSTRACT

In this paper, a high-resolution visualization technique has been used in combination with an extensively validated 0D model in order to relate the external structure of a diesel spray to the internal properties in the vicinity of the nozzle. For this purpose, three single-hole convergent nozzles with different diameters have been tested for several pressure conditions. The analysis of the obtained images shows that the spray width significantly changes along the very first millimeters of the spray. From the high resolution images captured, two parameters have been evaluated. The first one is the external non-perturbed length, where droplet detachment has not been observed. The second one is a transitional length, defined as the axial position where the spray width increases linearly after a transient behavior, making it possible to establish a spray cone angle definition. Furthermore, the internal liquid core length has been estimated for these nozzles using an extensively validated zero-dimensional model. The intact liquid core length has proved to be correlated with both the transitional length and the non-perturbed length with a very high degree of reliability. In the case of the transitional length, a quadratic correlation has been observed, whereas a linear relationship has been confirmed between the intact core length and the non-perturbed length. The results presented here may help to shed light on better understanding of such a complex process as atomization.

KEYWORDS: Diesel spray, atomization, near-nozzle, high pressure injection, breakup length, intact liquid core.

1. INTRODUCTION

The knowledge of the atomization process in diesel sprays is valuable due to the fact that combustion efficiency and emissions are directly related to spray atomization and fuel-air mixing processes. During the last decade, several tools were developed aiming at the analysis of diesel spray behavior [1-8]. Nevertheless, due to the complexity of the problem, there are still a lot of uncertainties on spray formation and break-up. Research activities have been made in the last years to characterize sprays under high injection pressure conditions by using visualization techniques focused on the nozzle vicinity zone. In this sense, the authors analyzed the transient structures in the first millimeters of diesel sprays using different optical techniques [9]. They observed that, during the initial stage of the injection, the spray consists of a non-perturbed liquid column and an umbrella-shaped structure in the nozzle tip. Linne et al. [10] studied the first 3 millimeters of the spray identifying and evaluating periodic structures on the spray contour. Kastengren et al. [11, 12] used X-Ray techniques to measure the projected mass distribution up to the first 5 millimeters of the spray.

Spray atomization has also been assessed by using numerical simulations, either using a Reynolds-averaged Navier-Stokes (RANS) equations approach for turbulence modeling [13, 14] or even using direct numerical simulations (DNS) [15, 16, 17] despite the high computational cost of this kind of simulations. Som et al. [13] showed the differences in the combustion process between two breakup models: the KH model and the KH-ACT model, which consists of an improvement to the KH model by also considering cavitation and turbulence phenomena. The inclusion of these improvements enhanced the primary breakup process, causing smaller droplet sizes and a decrease in liquid penetration. With regard to the flame lift-off length, the KH-ACT model predicted a lift-off length closer to the experimental values. Shinjo et al. [15, 16] and Ménard et al. [17] studied the diesel spray at low injection velocity. In [15, 16], the formation of ligaments and droplets was studied at 30, 50 and 100 m/s. Lebas et al. [14] used the DNS calculations of Menard et al. [17] to set the parameters and constants of an ELSA (Eulerian-Lagrangian Spray Atomization) model, which was successfully tested with experimental data in terms of liquid and vapor penetration.

It is well known that spray characteristics are highly influenced by the flow features at the nozzle outlet [18, 19, 20, 21]. However, their study is very complicated due to the small orifice diameters, the high velocities and the cavitation phenomenon that can take place inside the nozzle, especially in non-convergent nozzles [22, 23, 24, 25, 26]. Additionally, many researchers have observed an important increase in the atomization level and the spray angle connected to cavitation phenomenon [5, 19, 24, 27, 28].

In the present paper, the atomization process of Diesel sprays has been assessed by visualizing the spray in the first millimeters. To this end, three single-hole convergent nozzles with different diameters have been tested for a wide range of pressure conditions. The tests have been carried out with a diffused backlighting technique, performing the acquisition at two different image resolutions in order to focus in different regions of spray. With all, the study region ranges from the nozzle tip to 5.5 mm away in the axial direction.

Two different parameters have been evaluated. The external non-perturbed length has been obtained from the best resolution images, whereas a transitional length indicating the axial position after an initial transient zone from which the spray width spreads linearly with the axial position has been determined from the lowest resolution images. From this transitional length onwards, a spray cone angle definition can be established if the droplets in the border of the spray with axial position higher than the transitional length are used. In parallel, the potential of a 0-dimensional model previously validated for a wide range of conditions has made it possible to characterize the internal liquid core for the different injection conditions tested on these nozzles. This parameter, which is not experimentally accessible with the optical technique used in this investigation, has been compared and correlated with the non-perturbed length and the transitional length.

The paper is divided into 5 sections. In Section 2, the visualization facility, the optical setup and the technique used to process the images have been described. Section 3 includes the results and analysis of the images taken from visualization. Afterwards, a theoretical model for the liquid core length is obtained in Section 4, where the results from this model are also compared with previous experimental results in order to link both the internal and external parameters in a spray. Finally, the most important conclusions of the study have been pointed out in Section 5.

2. EXPERIMENTAL TOOLS

A Bosch common-rail fuel injection system with a solenoid-valve operated injector has been used. A standard commercial diesel fuel has been chosen for the study. The main physical and chemical characteristics of this fuel are reported in Table 1.

2.1 Determination of the internal geometry of the nozzles

A methodology based on silicone molding [29] has been employed to get information on the internal geometry of the nozzles used. The results of the values obtained applying this technique are displayed in Table 2, in which the values of diameter at the inlet and at the outlet of the nozzle are shown. As it can be noted, the three nozzles are strongly conical and therefore not prone to cavitate [19]. The degree of conicity of each nozzle is evaluated by means of the *k-factor*, defined as:

$$k - factor = \frac{D_i[\mu m] - D_o[\mu m]}{10} \quad (1)$$

2.2 Visualization setup

The tests have been carried out with a diffused backlighting technique combined with an optical setup that includes a biconvex lens, making it possible to achieve high amplification ratios. A scheme of this optical setup is shown in Fig. 1. As it can be seen, the laser source used for illumination and the CCD camera are placed in opposite sides of the visualization test rig. The laser, the camera and the lens are aligned. A specific drawing of the visualization test rig is shown in Fig. 2. It mainly consists of a stainless steel cylinder with two optical windows. The upper cover contains the injector holder, whereas the cover in the bottom contains the backpressure regulation system, which makes use of N_2. The maximum pressure in the chamber is limited to 6 MPa due to mechanical tolerances. A Nd-YAG laser operating in pulsed mode has been used as an illumination source since it offers the possibility of using small shot duration (around 7 ns), which is needed to freeze the image and capture the structures of the spray. The purpose of the optical diffuser placed after the laser (Fig. 1) is to produce uniform illumination and to filter the high intensity, avoiding damages in the camera sensor. The facility makes it possible to set the distances between the camera, lens and test rig in order to get the pictures with the desired magnification ratio. These distances depend on the size of the required visualization window, the characteristics of the lens, the size of the CCD sensor and the refractive index of the fluid that fills the visualization chamber.

The characteristics of the lens are displayed in Table 3. These magnitudes are related to the following equations:

$$\frac{1}{d_1} + \frac{1}{d_2} = \frac{1}{FL} \qquad (2)$$

$$M = \frac{h_s}{h_w} = \frac{d_2}{d_1} \qquad (3)$$

where FL is the focal length, d_1 is the distance from the spray axis to the lens, d_2 is the distance from the CCD sensor to the lens, M is the magnification ratio, h_w is the size of the visualization window and h_s is the camera sensor size (=7 mm.). The distances used in the current investigation for both configurations are displayed in Table 4.

2.3 Experimental methodology and acquired image processing

As it has been mentioned, an optical facility has been used for visualizing Diesel sprays at steady conditions, injecting in a pressurized chamber. With this aim, a set of 20 pictures has been acquired at the time instant that corresponds to full needle-lift conditions, so that the flow characteristics are stabilized. Two picture resolutions have been used: 250 pixels/mm (visualization window of 4.2x5.5 mm) and 1000 pixels/mm (visualization window of 1.2x1.5 mm). The first resolution level has made it possible to characterize the external spray morphology up to about 5.5 millimeters, and it has been used to analyze the evolution of spray width. The second one has been useful to obtain more specific information of the spray structure in the first 3 mm of the spray.

An injection pressure of 50 MPa has been tested for different values of chamber density, which has been modified by controlling the chamber pressure. The values of chamber pressure and their corresponding densities are shown in Table 5.

Pictures obtained from the visualization tests have been processed using an on-purpose software developed and implemented in Matlab. This software uses an algorithm based on Otsu's method [30] to detect the intensity threshold that defines the spray. This method has proved to be useful for pictures that clearly show two regions (liquid and gas) with different intensity levels [1, 6, 18, 19, 20, 21]

3. EXPERIMENTAL RESULTS AND ANALYSIS

Fig. 3 shows two samples of the pictures acquired for the highest resolution configuration. They belong to nozzles A and C at an injection pressure of 50 MPa and a chamber pressure of 1 MPa. This resolution allows the visualization of the first 1.5 mm of the spray. These images are analyzed afterwards, but at first glance it can be seen that there is a region near the nozzle where the spray width is practically constant and equal to the outlet diameter. Additionally, it can be seen that this region is longer for the Nozzle C, which has a larger nozzle diameter.

Fig. 4 displays two samples of pictures using the lowest resolution. This kind of image makes it possible to visualize the spray up to a distance of around 5 mm from the nozzle in the axial direction. These images belong to the nozzle A, at the injection pressure of 50 MPa and two different backpressures of 1 MPa (left) and 2.5 MPa (right). In this case, it can be clearly noted that an increase in the chamber pressure leads to a higher spray width due to the influence of chamber density on the air-fuel mixing process.

The spray width has been determined by the images processing algorithm. Its axial evolution has been analyzed for all the nozzles and experimental conditions tested in order to study the near-nozzle field structure. As a sample, the contour obtained for

Nozzle A for the backpressure of 1 MPa is displayed in the bottom part of Fig. 5. Additionally, a linear fit applied to the spray contour points located far from the nozzle is depicted as a solid line. According to the contour shape, it is possible to distinguish three different zones in the spray:

- Zone 1 (until ~0.4 mm): the spray width is constant and equal to the nozzle outlet diameter. It defines the non-perturbed length (L_{np}).
- Zone 2 (from ~0.4 mm until ~2.2mm): atomization takes place and the evolution of spray width with the axial position is not linear. The distance from the nozzle to the end of this zone is called transitional length (L_t).
- Zone 3 (from ~2.2 mm onwards): the contour profile follows a linear fit with high accuracy.

As shown in the upper part of Fig. 5, in addition to the transitional length and the non-perturbed length, there is a third parameter related to the internal liquid core length, L_c. This parameter is not possibly determined by the visualization technique carried out in this investigation. Other techniques might be used in order to assess this internal characteristic length, such as X-ray measurements [11, 12]. In the current study, a 0-dimensional model able to predict the liquid core length and the axial velocity drop along the spray axis has been used in order to compare the intact liquid core length with the non-perturbed length and the transitional length experimentally determined. This model has been previously validated using Particle Doppler Anemometry [31] and X-ray measurements of mass distribution in the primary break-up zone of the spray [7, 8].

In order to precisely characterize the non-perturbed length, the pictures with the best resolution have been used. The transitional length and the spray cone angle have been determined using the lowest resolution pictures.

3.1. Spray cone angle analysis

The spray cone angle is normally used to assess the efficiency of the mixing process. Its value is mainly dependent on nozzle geometry [18], the presence or absence of cavitation phenomenon [5, 19] and chamber density [21, 31, 32, 33]. This parameter is usually determined taking the assumption that the spray is similar to a cone, performing a linear fit to both the upper and the lower parts of the spray contour and determining the angle formed by both lines. However, this fit would only be accurate from the transition length onwards. To solve this problem, the contour is treated as shown in Fig. 6. It is first divided in segments of 50 pixels, starting from the end of the image. From these segments, a series of b_i vectors is defined, including the coordinates of the contour points corresponding to each of the segments in a cumulative way (i.e. the b_1 vector includes the points of the first segment of the contour, the b_2 vector includes the ones corresponding to the first and the second segment, and so on). With the information of each vector it is possible to obtain a linear fit over both the upper and the lower side of the spray contour, making it possible to calculate the angle among both. While the spray contour exhibits a conical shape, the error when performing both linear fits will diminish as the number of segments increases, since more points will be available. However, when the spray appearance deviates from this linear trend, the associated error to the linear fits will increase. Thus, the spray angle is taken as the one defined by the segment that leads to a lower error when performing the linear fit.

The evolution of spray cone angle against chamber density (ρ_a) is represented in Fig. 7 for all the nozzles. Measurements are displayed with the standard deviation. As expected, the higher the air density in the chamber, the higher the spray cone angle. This is due to aerodynamic interaction between the fuel and the air in the chamber. Regarding the comparison between the different nozzles, neither significant nor clear influence of the nozzle diameter on the spray cone angle can be confirmed.

3.2. Non-perturbed length and transitional length

As it has been mentioned, the spray shows an initial region at which the spray width is constant, which has been defined as non-perturbed length (L_{np}). The values of non-perturbed length for all the nozzles and the different backpressures tested are displayed in the bottom part of Fig. 8. A decrease on this parameter when chamber density increases can be noted, due to the effect of the aerodynamic forces on the primary atomization process. A significant and clear influence of the nozzle diameter on the non-perturbed length is noticed, as opposed to the spray cone angle results previously exposed: the higher the nozzle diameter, the higher the non-perturbed length. Therefore, the highest values of L_{np} are seen for Nozzle C, followed by Nozzle B, whereas the lowest values are observed for Nozzle A. As far as the transitional length is concerned, the values obtained from the analysis of the images are depicted against chamber density in the upper part of Fig. 8. As it can be observed, it exhibits a similar trend against density as the one observed for the non-perturbed length. Thus, the transitional length decreases as chamber density increases as a consequence of its effect on atomization and air-entrainment processes. Additionally, it is noticeable that the nozzle outlet diameter has a strong influence on transitional length, showing a similar trend as the one seen for the non-perturbed length. If both parameters are compared for a given density (chamber pressure) it can be seen that the transitional length values are higher than the non-perturbed length ones, although they have the same order of magnitude.

4. MODEL FOR LIQUID CORE LENGTH AND RELATION WITH PREVIOUS EXPERIMENTALLY DETERMINED PARAMETERS.

4.1 Theoretical derivation.

The model is obtained under the hypothesis of momentum flux conservation along the spray axis. This hypothesis was validated using momentum measurements [1], and it implies that:

$$\dot{M}_o = \dot{M}(x) \tag{4}$$

where $\dot{M}(x)$ and $\dot{M}_o$ are the momentum flux at a section at a distance x from the nozzle tip in the axial direction and the momentum flux at the orifice outlet, respectively. Momentum flux at the nozzle outlet is defined as:

$$\dot{M}_o = \dot{m}_f \cdot U_o \tag{5}$$

If Eq. (4) is integrated over the whole spray section, it can be written as:

$$\dot{M}_o = \dot{M}(x) = \int_0^\infty 2\pi\rho(x,r)\, r U^2(x,r)\, dr \tag{6}$$

where the x-coordinate follows the axial direction and the r-coordinate is perpendicular to the spray axis. In Eq. (6), $U(x,r)$ is the local spray velocity and $\rho(x,r)$ is the local density. If a Gaussian profile is assumed for both fuel concentration and axial velocity, the integration of Eq. (6) leads to Eq. (7). It is important to remark at this point that the

Gaussian profile has proved to be suitable to explain the radial distributions of concentration and velocity in Diesel sprays [1, 5, 7, 8, 31, 34].

$$\dot{M}_o = \frac{\pi}{2\alpha}\rho_a \tan^2\left(\frac{\theta_u}{2}\right) x^2 U_{axis}^2 \sum_{i=0}^{\infty} \frac{1}{\left(1+i\,\frac{Sc}{2}\right)} \left[C_{axis}(x)\left(\frac{\rho_f-\rho_a}{\rho_f}\right)\right]^i \tag{7}$$

All the steps followed in the integration of Eq. (6) can be found in Desantes et al. [35].

In Eq. (7), ρ_a and ρ_f are the air density and the fuel density, respectively, whereas α is the shape parameter of the Gaussian profile and Sc is the effective Schmidt number, which is defined as the ratio of momentum diffusivity to mass diffusivity:

$$Sc = \frac{\nu}{D} \tag{8}$$

being D the mass diffusivity and ν the kinematic viscosity.

The spray velocity angle θ_u is defined by the points in the border of the spray at which velocity drops 1% of its value at the spray axis for the same axial coordinate.

This model was extensively validated in previous studies [31, 35], both in terms of local velocity and local mass concentration, by means of spray momentum flux measurements and PDA (phase doppler anemometry) measurements, among others.

The momentum flux at the nozzle outlet can also be defined as:

$$\dot{M}_o = \rho_f A U_o^2 \tag{9}$$

where A is the area of the nozzle orifice at the outlet and U_o is the effective injection velocity at this location. Substituting Eq. (9) in Eq. (7), it can be easily transformed into:

$$\rho_f A = \frac{\pi}{2\alpha}\rho_a \tan^2\left(\frac{\theta_u}{2}\right)x^2\left(\frac{U_{axis}}{U_o}\right)^2 \sum_{i=0}^{N}\frac{1}{\left(1+i\,\frac{Sc}{2}\right)}\left[C_{axis}(x)\left(\frac{\rho_f-\rho_a}{\rho_f}\right)\right]^i \tag{10}$$

where N is the number of terms used in series truncation. Previous studies show that axial concentration and velocity can be related in terms of Schmidt number [36] as:

$$\left(\frac{U_{axis}(x)}{U_o}\right) = C_{axis}(x)^{Sc} \tag{11}$$

If Eq. (11) is introduced in Eq. (10), an implicit equation for C_{axis} as a function of Sc can be obtained:

$$1 = \frac{\pi}{2\alpha}\frac{\rho_a}{\rho_f}\frac{1}{A}\tan^2\left(\frac{\theta_u}{2}\right)x^2\left(C_{axis}(x)\right)^{2Sc}\sum_{i=0}^{N}\frac{1}{\left(1+i\,\frac{Sc}{2}\right)}\left[C_{axis}(x)\frac{\rho_f-\rho_a}{\rho_f}\right]^i \tag{12}$$

Finally, considering that the spray mass angle (θ_m) is related to the spray velocity angle (θ_u) through the following equation:

$$\tan\left(\frac{\theta_u}{2}\right) = \sqrt{Sc}\,\tan\left(\frac{\theta_m}{2}\right) \tag{13}$$

and introducing Eq. (13) in Eq. (12), the following expression is obtained:

$$1 = \frac{\pi}{2\alpha}\frac{\rho_a}{\rho_f}\frac{1}{A}Sc\tan^2\left(\frac{\theta_m}{2}\right)x^2\left(C_{axis}(x)\right)^{2Sc}\sum_{i=0}^{N}\frac{1}{\left(1+i\,\frac{Sc}{2}\right)}\left[C_{axis}(x)\frac{\rho_f-\rho_a}{\rho_f}\right]^i \tag{14}$$

In previous works by the authors [7, 8], projected mass distributions obtained from experiments based on X-ray absorption were transformed into mass concentration in the axis for different nozzles and conditions and compared to the results provided by this model (Eq. 14). As a sample of this procedure, Fig. 9 shows a comparison among the mass concentration in the axis and the mass concentration predicted by the model for different Sc numbers between 0.5 and 1. The filled circles represent the values reconstructed from X-ray measurements following the procedure explained in [7, 8]. This measurement belongs to a nozzle with orifices of 131 µm of diameter and P_{inj} = 80 MPa and P_b = 1.85 MPa (ρ_a = 21 kg/m^3).

As it can be noted, Sc has an important influence on C_{axis} evolution until an axial position of 75-80 D_o (~10-12 mm), where the difference between the curves becomes almost indiscernible. As can be seen, attending to the behavior of C_{axis}, two different zones can be defined. From 30 D_o (i.e. ~4 mm) onwards, the axial concentration is well reproduced by the theoretical model for Sc = 0.5. On the contrary, for positions up to nearly 30 D_o, C_{axis} does not follow any specific theoretical curve. This is mainly due to fact that, as reported in Section 3, the spray cone angle near the nozzle outlet (in the zone close to the intact core length) is not well established (see results depicted in Fig. 6). Despite this limitation of the model, as shown in Fig. 9, a very good estimation of the intact core length (further point in the axis with C_{axis} = 1) can be obtained using the 0-D model when Sc number equals the unity. This result was also observed for other different nozzles and conditions in previous investigations [7, 8] using X-ray measurements. Thus, in this situation (Sc = 1), it is possible to obtain an explicit expression for the intact liquid core length (L_c). Indeed, particularizing Eq. (14) for Sc = 1 and $C_{axis}(x)$ = 1, the following expression is obtained for $x = L_c$:

$$L_c = \frac{\left(\frac{\alpha}{2}\right)^{1/2} \cdot D_{eq}}{tan\left(\frac{\theta_m}{2}\right)} \cdot \frac{1}{\left[\sum_{i=0}^{N} \frac{1}{\left(1+\frac{i}{2}\right)}\left[\left(\frac{\rho_f - \rho_a}{\rho_f}\right)\right]^i\right]^{1/2}} \qquad (15)$$

where the definition of equivalent diameter ($D_{eq} = D_o \sqrt{\rho_f / \rho_a}$) has been used, and the area A in Eq. (14) has been substituted by:

$$A = \frac{\pi \cdot D_o^2}{4} \tag{16}$$

Chehroudi et al. [37] found the following expression for the normalized liquid core length:

$$L_c / D_o = C_c \cdot (\rho_f / \rho_a)^{0.5} \tag{17}$$

being C_c an empirical constant in the range from 7 to 16. This expression, although simpler than Eq. (14), keeps the same dependency with the density ratio as the one expressed by Eq. (14) (if the definition of the equivalent diameter is taken into account).

In the next Section, the evaluation of the intact core length will be addressed for all the nozzles and operating conditions and it will be correlated with the previously examined external parameters (non-perturbed length and transitional length).

4.2 Evaluation of the intact core length and comparison with previous experimentally determined parameters.

The liquid core length can now be evaluated for the three nozzles and different injection conditions. In Fig. 10, the liquid core length evaluated by means of Eq. (15) has been depicted for all nozzles and densities in the chamber. As expected according to Eq. (15), there is a great influence of the chamber air density on the liquid core length: the higher the density, the higher the spray angle (as shown in Fig. 7), and therefore the shorter the liquid core length due to the enhanced air entrainment. As far as the influence of the orifice diameter is concerned, the higher the diameter, the longer the liquid core length, as can be clearly seen for all the conditions displayed in Fig. 10. The same conclusion is reached if the equivalent diameter is considered. It should be noted that, although the difference in the liquid core length between the three nozzles is reduced in absolute terms when increasing the chamber density, their differences in relative terms remain similar. This result was expected in the light of Eq. (15), due the differences in D_{eq} among nozzles and the fact that there is no clear influence of the nozzle on the spray angle, as pointed out in Section 3.1.

If results of intact core length are compared to the previous results of non-perturbed length and transitional length, it can be concluded that even though the intact core length is quite higher than both of them in overall terms, the intact core and the transitional length come closer for high densities. For instance, whereas the values for the liquid core, transitional length and non-perturbed length for nozzle 156 at 5.8 kg/m^3 of density are 12.5 mm, 2.8 mm and 0.85 mm, respectively, the values encountered for a density of around 60 kg/m^3 are 2 mm, 1.7 mm and 0.2 mm.

A non-dimensional intact liquid core length can be obtained by dividing this parameter by the equivalent diameter. This non-dimensional intact length has been depicted in the upper part of Fig. 11 against the normalized transitional length. As can be noted, there is a clear quadratic correlation among both parameters. The mathematical expression that better fits this relation is:

$$\frac{L_c}{D_{eq}} = 0.0199 \cdot \left(\frac{L_t}{D_{eq}} \right)^2 \qquad (18)$$

with a coefficient of determination R^2 equal to 0.99.

If the values of non-dimensional liquid core length are compared to the corresponding non-dimensional non-perturbed length, the results displayed in the bottom part of Fig. 11 are obtained. As can be noted, the dependency between both parameters is linear in this case, obtaining the following equation that relates them:

$$\frac{L_c}{D_{eq}} = 12.9245 \cdot \frac{L_{np}}{D_{eq}} \qquad (19)$$

with a coefficient of determination R^2 equal to 0.97.

The correlations obtained for the transitional length and non-perturbed length make it possible to determine the dependencies of those parameters with the equivalent diameter (including geometrical diameter, D_o, the fuel properties, ρ_f, and the density in the chamber, ρ_a) and the spray cone angle, $tan\left(\frac{\theta_m}{2}\right)$. Indeed, as established by Eq. (15), the liquid core length depends on the equivalent diameter and the spray cone angle as follows:

$$L_c \propto \frac{D_{eq}}{tan\left(\frac{\theta_m}{2}\right)} \qquad (20)$$

where the term involving the series in the denominator in Eq. (15) has been neglected as a first approximation and for simplicity reasons:

Taking into account Eq. (18), the transitional length can be written as:

$$\frac{L_t}{D_{eq}} \propto \sqrt{\frac{L_c}{D_{eq}}} \qquad (21)$$

and therefore:

$$L_t \propto \sqrt{D_{eq} \cdot L_c} \tag{22}$$

Introducing Eq. (20) into Eq. (22) yields:

$$\frac{L_c}{L_t} \propto \frac{1}{\sqrt{tan\left(\frac{\theta_m}{2}\right)}} \tag{23}$$

This last equation helps explaining the quadratic correlation observed in Fig. 11 (upper part): for lower chamber densities (and therefore smaller spray cone angles), differences between both parameters become higher, whereas for higher chamber densities (and therefore bigger spray cone angles), the differences become smaller. Table 6 shows a comparison among the values of $1\Big/\sqrt{tan\left(\frac{\theta_m}{2}\right)}$ and the values of the ratio L_c/L_t for all the nozzles and density conditions, using the previously experimentally (L_t) and theoretically derived (L_c) values. As can be noted, even though both values differ because Eq. (23) only shows a proportional relationship, they show a similar trend when moving from low densities to high densities.

With regard to the non-perturbed length, a linear correlation was found between L_{np} and L_c (recall Eq. (19)). Thus, carrying out a similar procedure to the one previously described for the transitional length would lead to the conclusion that the dependencies of this parameter with the equivalent diameter and spray cone angle are the same as in the case of the liquid core length, i.e.:

$$L_{np} \propto \frac{D_{eq}}{tan\left(\frac{\theta_m}{2}\right)}$$

5. CONCLUSIONS

In the current paper, a visualization technique has been used to study the stationary spray structure in the vicinity of the nozzle. Two different levels of image resolution have been obtained: a visualization window of around 5 mm from which the axial evolution of spray width has been characterized, and a window of 1.5 mm that has made it possible to evaluate the external non-perturbed length. A qualitative analysis of the spray contour has shown the existence of three different zones in the spray attending to the axial evolution of the spray width: a first zone, where spray width is equal to the nozzle outlet diameter; a second zone, called transitional zone, at which air-entrainment has already begun but where the evolution of spray width is not linear; and a third zone (or steady-state region) characterized by a linear spray width evolution defined by a steady spray cone angle value.

Spray cone angle has shown to be similar for the three nozzles tested, with a significant influence of the density. No clear dependency with the nozzle outlet diameter has been observed. With regard to the non-perturbed length, it has been seen that it decreases when chamber density increases due to the effect of aerodynamic forces on the primary atomization process. In this case, there is a significant and clear influence of the diameter on the non-perturbed length: the higher the diameter, the higher the non-perturbed length. The transitional length (axial distance from the nozzle outlet at which the spray width starts its linear evolution) has shown a similar behavior as the non-perturbed length, but with higher values.

An equation for the liquid core length has been derived using a previously validated model. According to this model, the liquid core length depends mainly on the air density (or more generally the fuel/air density ratio) and the nozzle diameter. For all the nozzles and conditions, the liquid core length has exhibited the highest values for the nozzle with the highest diameter for the lowest air density in the chamber, whereas it has shown the lowest values for the nozzle with the lowest diameter for the highest air density in the chamber. The estimated values of liquid core length have been compared with the experimentally obtained transitional length and non-perturbed length values. As a result of the comparison, the non-dimensional liquid core length (normalized using the equivalent diameter) has shown to correlate with a very high level of confidence (R^2= 0.99) with the non-dimensional transitional length. In this case, a quadratic equation has been found to be the best approach to describe the relationship among both parameters. On the other hand, when comparing the non-dimensional liquid core length with the external non-perturbed length, a linear relationship between them has been found. Again, the coefficient of determination found is close to 1, highlighting the potential of the correlation for predicting the liquid core length from the non-perturbed length, or vice versa.

The analysis of the obtained correlations allows to conclude that the ratio among the transitional length and the liquid core length is proportional to the square root of the half-angle tangent. This result would explain the quadratic correlation found among both parameters. In the case of the non-perturbed length, the dependency with the equivalent diameter and the angle is exactly the same as the one for the liquid core length.

Acknowledgements

This work was funded by "*Ministerio de Economía y Competitividad*" of Spanish Government, in the frame of the Project "Comprensión de la influencia de combustibles no convencionales en el proceso de injección y combustión tipo Diesel" (Reference TRA2012-36932).

REFERENCES

1. Desantes, J.M., Payri, R., Salvador, F.J., Gil, A., Development and validation of a theoretical model for Diesel spray penetration. Fuel, vol. 85, pp. 910-917, 2006.
2. Kim, H.J., Park, S.H., Lee, C.S., A study on the macroscopic spray behaviour and atomization characteristics of biodiesel and dimethyl ether sprays under increased ambient pressure. Fuel Processing Technology, vol. 91(3), pp. 354-363, 2010.
3. Klein-Douwel, R.J.H., Frijters, P.J.M., Seykens, X.L.J., Somers, L.M.T., Baert, R.S.G., Gas density and rail pressure effects on Diesel spray growth from a heavy-duty common rail injector. Energy & Fuels, vol. 23(Sp. Iss), pp. 1832-1842, 2009.
4. Lee, C.S, Lee, K.H., Reitz, R.D., Park, S.W., Effect of split injection on the macroscopic development and atomization characteristics of a Diesel spray injected through a common-rail system. Atomization and Sprays, vol. 16(5), pp. 543-562, 2006.
5. Desantes, J.M., Payri, R., Salvador, F.J., De la Morena, J., Influence of cavitation phenomenon on primary break-up and spray behavior at stationary conditions. Fuel, vol. 89, pp. 3033-3041, 2010.
6. Payri, R., Salvador, FJ, Gimeno, J., Soare, V., Determination of Diesel sprays characteristics in real engine in-cylinder air density and pressure conditions. Journal of Mechanical Science and Technology, vol. 19, pp. 2040-2052, 2005.
7. Desantes, J. M., Salvador, F. J., López, J. J., De la Morena. J., Study of mass and momentum transfer in Diesel sprays based on X-ray mass distribution

measurements and on a theoretical derivation. Experiments in Fluids, vol. 50(2), pp. 233–246, 2011.

8. Salvador, F. J., Ruiz, S., Gimeno, J., De la Morena, J., Estimation of a suitable Schmidt number range in Diesel sprays at high injection pressure. International Journal of Thermal Sciences, vol. 50, pp. 1790–1798, 2011.
9. Hattori, H., Naruyima, K., Tsue, M., Kadota, T., Analysis of initial break-up mechanism of Diesel spray injected into high-pressure ambience. SAE Paper 2004-01-0528, 2004.
10. Linne, M.A., Paciaroni, M. Berrocal, E., Sedarsky, D., Ballistic imaging of liquid break-up processes in dense sprays. Proceedings of the Combustion Institute, vol. 32, pp. 2147-2161, 2009.
11. Kastengren, A., Tilocco, F.Z., Duke, D.J., Powell, C.F., Moon, S., Zhang, X., Time-resolved X-ray radiography of sprays from engine combustion network Spray A Diesel Injectors. Atomization and Sprays, vol. 24(3), pp. 251-272, 2014.
12. Kastengren, A., Powell, C.F., Synchrotron X-Ray techniques for Fluid Dynamics. Experiment in Fluids, vol. 55, pp. 1686, 2014.
13. Som, S., Aggarwal, S.K., Effects of primary breakup modeling on spray and combustion characteristics of compression ignition engines. Combustion and Flame, vol. 157(6), pp. 1179-1193, 2010.
14. Lebas, R., Menard, T., Beau, P.A., Berlemont, A., Demoulin, F.X., Numerical simulation of primary break-up and atomization: DNS and modeling study. International Journal of Multiphase Flow, vol. 35(3), pp. 247-260, 2009.
15. Shinjo, J., Umemura, A., Simulation of liquid jet primary breakup: dynamics of ligament and droplet formation. International Journal of Multiphase Flow, vol. 36(7), pp. 513-532, 2010.

16. Shinjo, J., Umemura, A., Detailed simulation of primary atomization mechanisms in Diesel jet sprays (isolated identification of liquid jet tip effects). Proceedings of the Combustion Institute, vol. 33(2), pp. 2089-2097, 2011.
17. Ménard, T., Tanguy, S., Berlemont, A., Coupling level set/VOF/ghost fluid methods: Validation and application to 3D simulation of the primary break-up of a liquid jet. International Journal of Multiphase Flow, vol. 33(5), pp. 510-524, 2007.
18. Bermúdez, V., Payri, R., Salvador F.J., Plazas, A.H., Study of the influence of nozzle seat type on injection rate and spray behaviour. Proceedings of the Institution of Mechanical Engineers, Part D: Journal of Automobile Engineering, vol. 219, pp. 677-689, 2005.
19. Payri F., Bermúdez V., Payri R., Salvador F.J., The influence of cavitation on the internal flow and the Spray characteristics in Diesel injection nozzles. Fuel, vol. 83, pp. 419-431, 2004.
20. Payri, R., Molina, S., Salvador, F.J., Gimeno, J., A study of the relation between nozzle geometry, internal flow and sprays characteristics in Diesel fuel injection systems. KSME International Journal, vol. 18, pp. 1222-1235, 2004.
21. Salvador, F.J., Ruiz, S., Salavert, J., De la Morena, J., Consequences of using biodiesel on the injection and air-fuel mixing processes in Diesel engines. Proceedings of the Institution of Mechanical Engineers, Part D: Journal of Automobile Engineering, vol. 227, pp. 1130-1141, 2013.
22. Luján, J.M., Tormos, B., Salvador, F.J., Gargar, K., Comparative analysis of a DI Diesel engine fuelled with biodiesel blends during the European MVEG-A cycle: Preliminary study (I). Biomass & Bioenergy, vol. 33, pp. 911-947, 2009.

23. Salvador, F.J., Romero, J.-V., Roselló, M.-D., Martínez-López, J., Validation of a code for modelling cavitation phenomena in Diesel injector nozzles. Mathematical and Computer Modelling, vol. 52, pp. 1123-1132, 2010.
24. Andriotis, A., Gavaises, M., Influence of vortex flow and cavitation on near-nozzle Diesel spray dispersion angle. Atomization and Sprays, vol. 19(3), pp. 247-261, 2009.
25. Salvador. F.J., Hoyas, S., Novella, R., Martínez-López, J., Numerical simulation and extended validation of two-phase compressible flow in Diesel injector nozzles. Proceedings of the Institution of Mechanical Engineers, Part D: Journal of Automobile Engineering, vol. 225, pp. 545-563, 2011.
26. Salvador, F.J., Martínez-López, J., Caballer, M., de Alfonso, C., Study of the influence of needle lift on the internal flow and cavitation phenomenon in Diesel injector nozzles by CFD using RANS methods. Energy Conversion and Management, vol. 66, pp. 246-256, 2013.
27. Hiroyasu, H., Spray breakup mechanism from the hole-type nozzle and its applications. Atomization and Sprays, vol. 10, pp. 511-527, 2000.
28. Sou, A., Hosokawa, S., Tomiyama, A., Effects of cavitation in a nozzle on liquid jet atomization. International Journal of Heat and Mass Transfer, vol. 50, pp. 3575-3582, 2007.
29. Macián, V., Bermúdez, V., Payri, R., Gimeno, J., New technique for determination of internal geometry of a Diesel nozzle with the use of silicone methodology, Experimental Techniques, vol. 27, pp. 39-43, 2003.
30. Otsu, N., A threshold selection method from gray-level histograms. IEEE Transactions on Systems, Man, and Cybernetics, vol. SMC-9, no. 1, pp. 62-66, 1979.

31. Payri, R. Tormos, B., Salvador, F.J., Araneo, L., Spray droplet velocity characterization for convergent nozzles with three different diameters. Fuel, vol. 87, pp. 3176–3182, 2008.
32. Delacourt, E., Desmet, B., Besson, B., Characterization of very high pressure Diesel sprays using digital imaging techniques. Fuel, vol. 84 (7-8), pp. 859-867, 2005.
33. Naber, J.D., Siebers, D.L., Effects of gas density and vaporization on penetration and dispersion of Diesel sprays. SAE paper 960034, 1996.
34. Yue, Y., Powell, C.F., Poola, R., Wang, J., Schaller, J.K., Quantitative measurements of Diesel fuel spray characteristics in the near-nozzle region using X-ray absorption. Atomization and Sprays, vol. 11(4), pp. 471-490, 2001.
35. Desantes, J.M., Payri, R., García, J.M., Salvador, F.J., A contribution to the understanding of isothermal Diesel spray dynamics. Fuel, vol. 86, pp. 1093-1101, 2007.
36. Desantes, J.M., Arrègle, J., López, J.J., Cronhjort, A., Scaling laws for the free turbulent gas jets and Diesel-like sprays. Atomization and Sprays, vol. 16, pp. 443-473, 2006.
37. Chehroudi, B., Onuma, Y., Chen, S.-H., Bracco, F.V., On the intact core of full-cone sprays. SAE Paper 850126, 1985.

TABLES AND FIGURE CAPTIONS

Table 1: Physical and chemical properties of Diesel fuel used in the experiments.

Test	Unit	Result	Uncertainty
Density at 15ºC	**Kg/m^3**	**843**	**±0.2**
Viscosity at 40ºC	**mm^2/s**	**2.847**	**±0.42**
Volatility			
65% distillated at	**ºC**	**294.5**	**±3.7**
85% distillated at	**ºC**	**329.2**	**±3.7**
95% distillated at	**ºC**	**357.0**	**±3.7**
Average fuel molecular composition		**$C_{13}H_{28}$**	

Table 2: Results for nozzles geometry by silicone moulding technique

Nozzle	D_i [μm]	D_o [μm]	*k-factor*
Nozzle A	140	112	2.8
Nozzle B	167	138	2.9
Nozzle C	195	156	3.9

Table 3: Biconvex lens characteristics

Focal length (*FL*)	100 mm
Lens diameter	50 mm
Material	BK7
Refractive index	1.52

Table 4: Distances between elements for the two optical configurations used

Visualization window[mm]	d_1 [mm]	d_2 [mm]
1.2 x 1.5	131	566
4.2 x 5.5	188	227

Table 5: Values of chamber pressure tested and their associated chamber densities.

Chamber pressure [MPa]	Chamber density [kg/m^3]
0.5	5.77
1.0	12.00
1.5	16.79
2.5	28.76
3.5	40.25
5.0	57.49

Table 6: Values of different spray parameters for all the nozzles.

Nozzle A		
ρ_a [kg/m^3]	$\frac{1}{\sqrt{\tan(\theta/2)}}$	$\frac{L_c}{L_t}$
5.77	4.31	5.38
11.99	3.34	2.74
16.79	3.20	2.34
28.76	3.04	1.98
40.25	2.72	1.72
Nozzle B		
ρ_a [kg/m^3]	$\frac{1}{\sqrt{\tan(\theta/2)}}$	$\frac{L_c}{L_t}$
5.77	3.86	4.47
11.99	3.42	3.09
16.79	3.21	2.43
28.76	2.81	1.61
40.25	2.62	1.37
Nozzle C		
ρ_a [kg/m^3]	$\frac{1}{\sqrt{\tan(\theta/2)}}$	$\frac{L_c}{L_t}$
5.77	3.84	4.69
11.99	3.39	3.02
16.79	3.22	2.51
28.76	2.81	1.67
40.25	2.71	1.59

FIGURE CAPTIONS

Figure 1: Experimental setup for near-nozzle field visualization.

Figure 2: Near-nozzle field visualization test rig.

Figure 3: Samples of images obtained from nozzles A and C with image resolution of 1.2 x 1.5 mm at an injection pressure of 50 MPa and backpressure of 1 MPa.

Figure 4: Samples of images obtained from nozzle A with image resolution of 4.2 x 4.5 mm at an injection pressure of 50 MPa and backpressures of 1MPa (left) and 2.5 MPa (right).

Figure 5: Parameters evaluated from the images of the spray: Non-perturbed length (L_{np}) and transitional length (L_t).

Figure 6: Spray angle determination method.

Figure 7: Spray angle as a function of the chamber density for the different nozzles.

Figure 8: Transitional length and non-perturbed length for different nozzles and density conditions.

Figure 9: Mass concentration in the axis of the spray: experimental and modeled for different Schmidt numbers. Liquid core length determination.

Figure 10: Intact core length as a function of density in the chamber.

Figure 11: Non-dimensional intact core length vs transitional length (upper part) and Non-dimensional intact core length vs external non-perturbed length (bottom part).

582 **FIGURES**

583

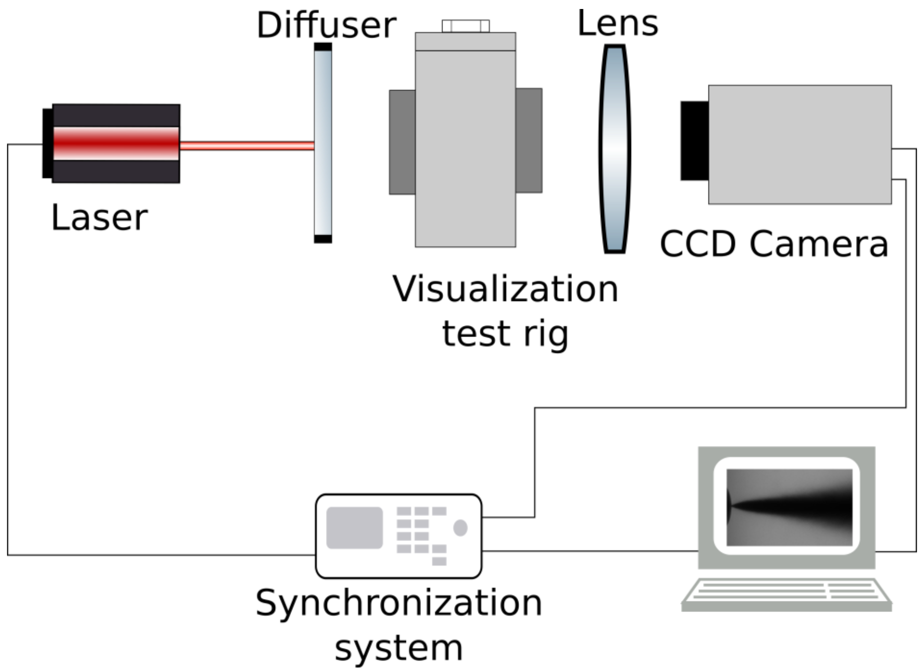

584

585 Figure 1: Experimental setup for near-nozzle field visualization

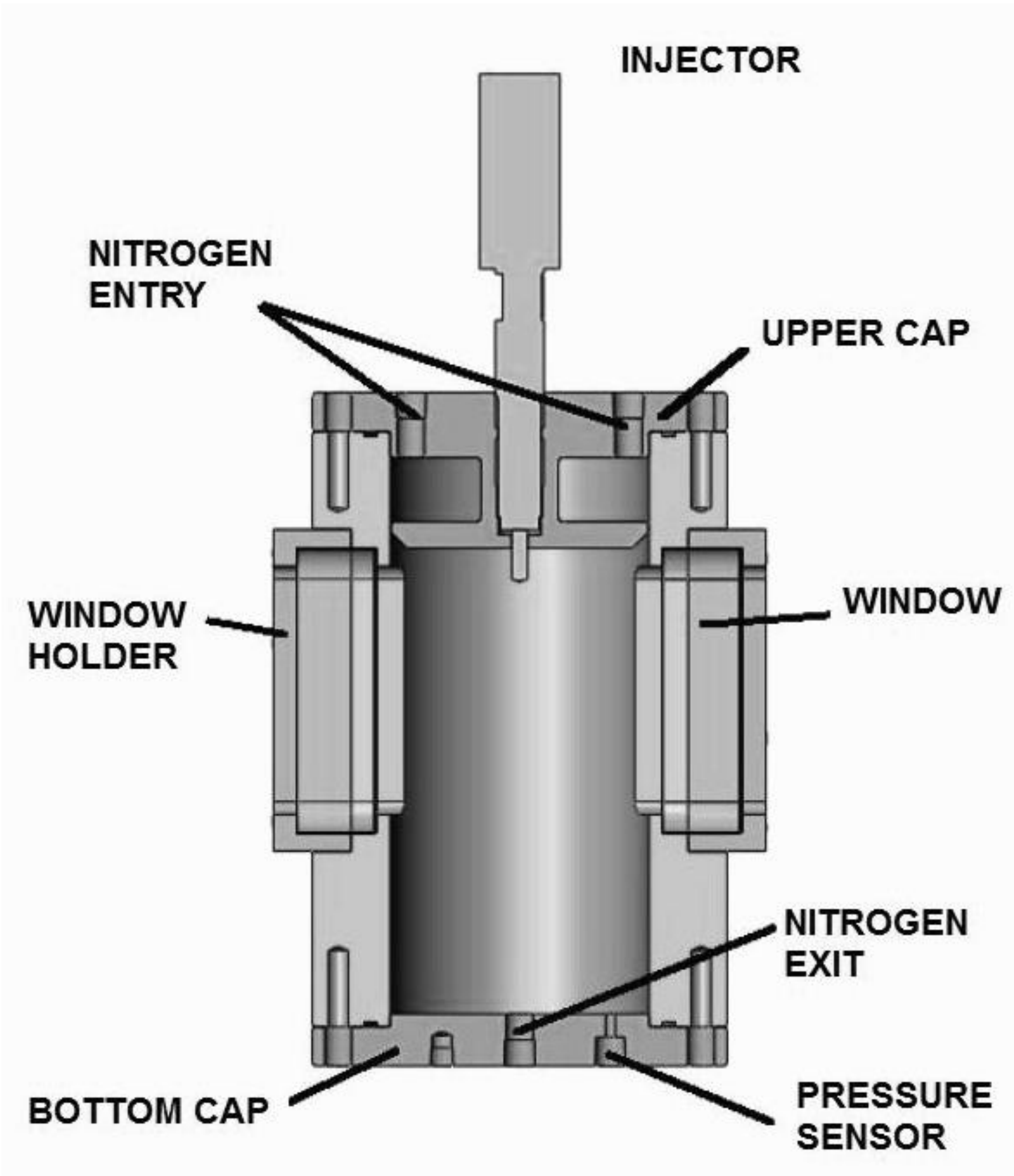

Figure 2: Near-nozzle field visualization test rig

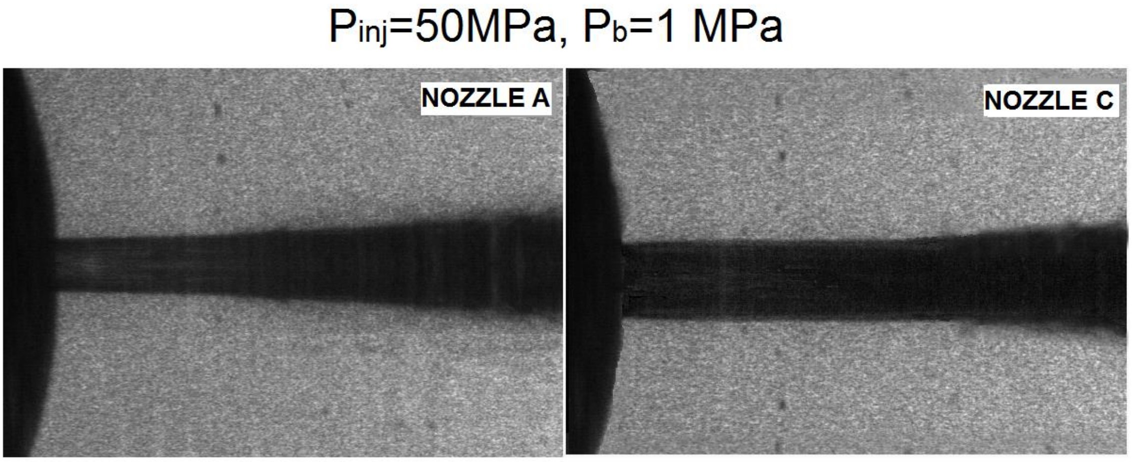

Figure 3: Samples of images obtained from nozzles A and C with image resolution of 1.2 x 1.5 mm at an injection pressure of 50 MPa and backpressure of 1 MPa.

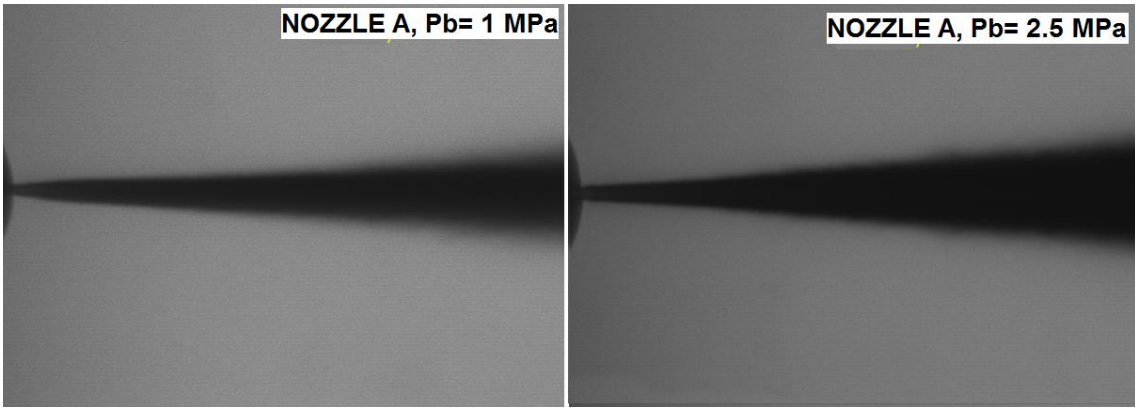

Figure 4: Samples of images obtained from nozzle A with image resolution of 4.2 x 4.5 mm at an injection pressure of 50 MPa and backpressures of 1MPa (left) and 2.5 MPa (right).

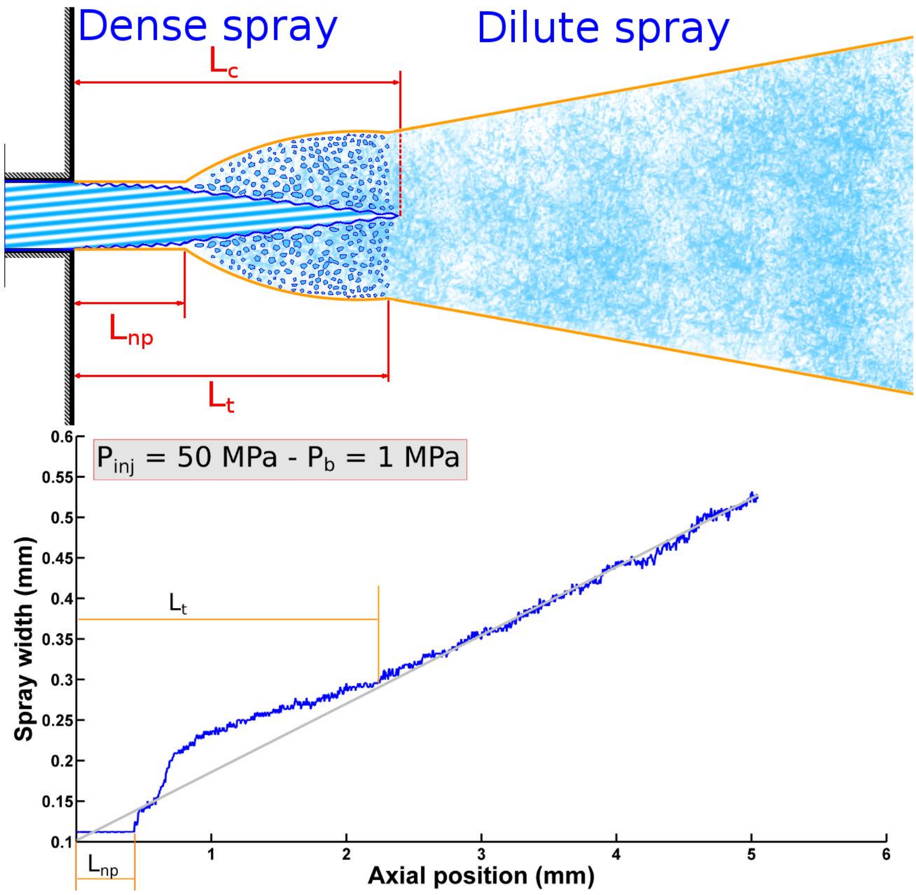

Figure 5: Parameters evaluated from the images of the spray: Non-perturbed length (L_{np}) and transitional length (L_t).

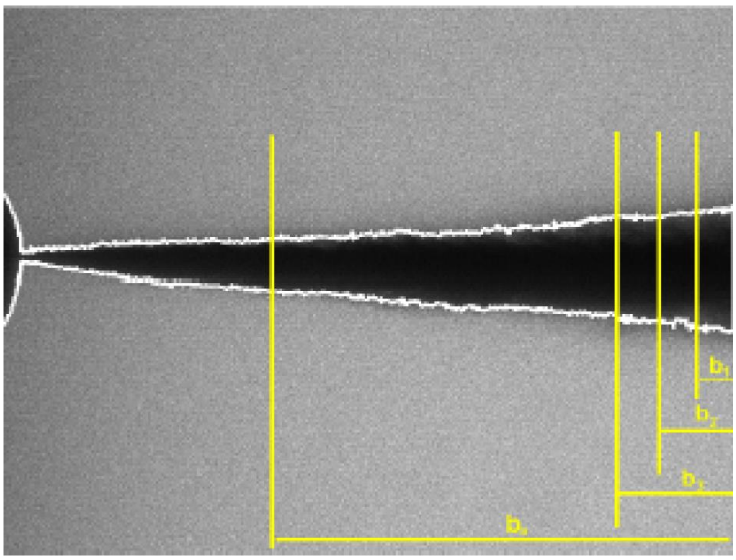

Figure 6: Spray angle determination method.

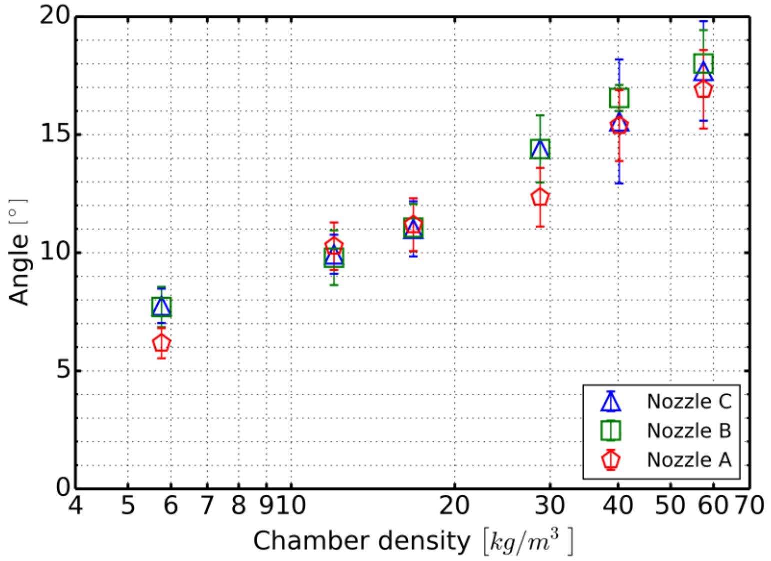

Figure 7: Spray angle as a function of the chamber density for the different nozzles.

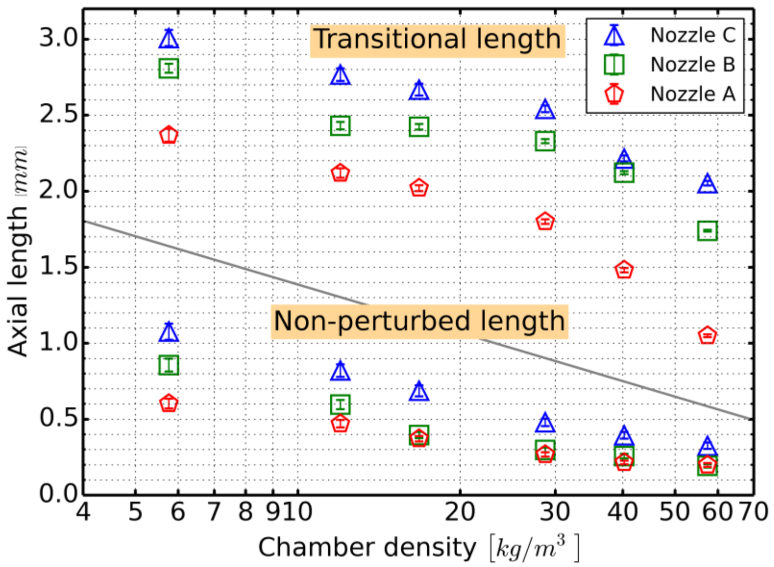

Figure 8: Non-perturbed length and transitional length for all the nozzles and density conditions.

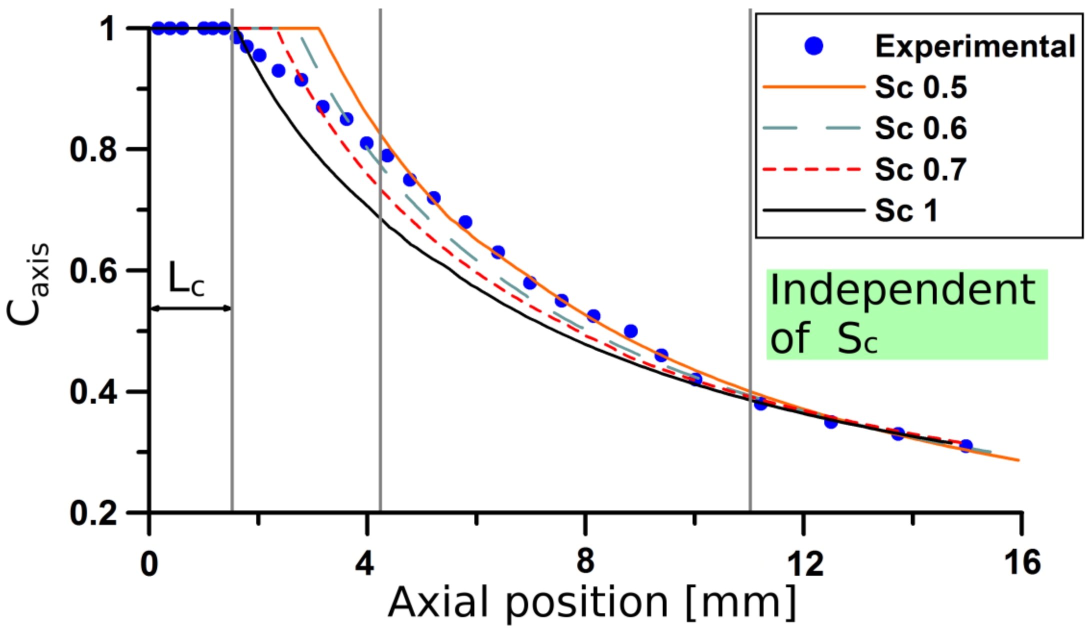

Figure 9: Mass concentration in the axis of the spray: experimental and modeled for different Schmidt numbers. Intact core length determination.

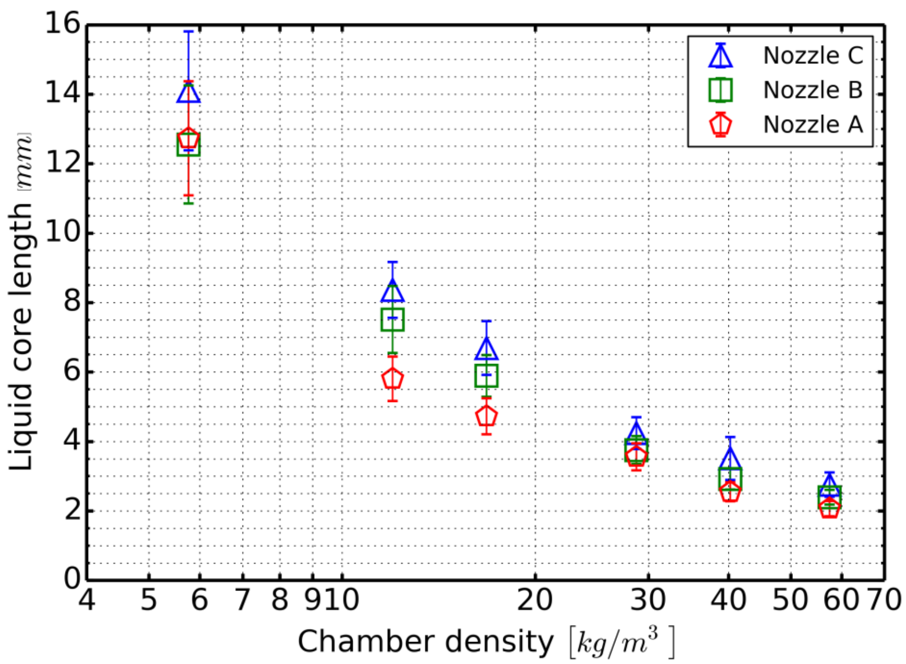

Figure 10: Intact liquid core length as a function of density in the chamber.

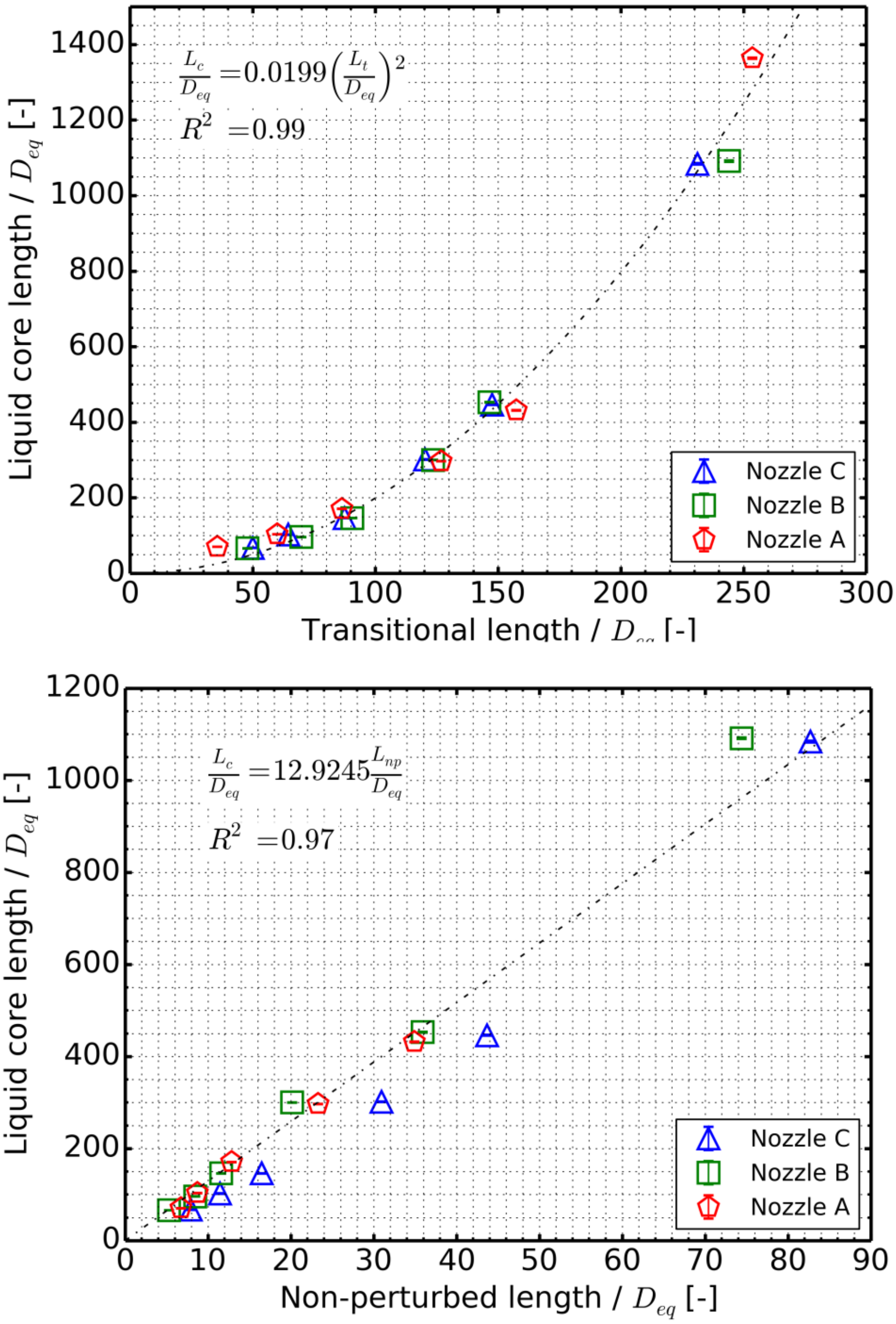

Figure 11: Non-dimensional intact liquid core length vs transitional length (upper part). Non-dimensional liquid intact core length vs external non-perturbed length. (bottom part).

NOMENCLATURE

A	Orifice outlet area
b_i	Vectors for the spray angle determination
C	Local fuel concentration
C_c	Empirical constant for the normalized liquid core length
D_{eq}	Equivalent diameter
D	Mass diffusivity
D_i	Diameter at the nozzle orifice inlet
D_o	Diameter at the nozzle orifice outlet
d_1	Distance from the spray axis to the lens
d_2	Distance from the lens to the camera sensor
FL	Lens focal length
h_s	CCD camera sensor length
h_w	Visualization window length
i	Counter for the series in the 0-D model
k-factor	Nozzle orifice conicity factor
L_c	Liquid core length
L_{np}	Non-perturbed length
L_t	Transitional length
$\dot{m}_f$	Mass flow rate
$\dot{M}_f$	Spray momentum flux
M	Magnification ratio for the visualization tests

P_{inj}	Injection pressure
P_b	Discharge pressure
Sc	Schmidt number
U_{axis}	Velocity in the axis of the spray
U_o	Effective velocity at the orifice outlet
Greek symbols:	
α	Shape parameter used in Gaussian distributions
θ_m	Spray angle from point of view of mass
θ_u	Spray angle from point of view of velocity
ρ_a	Density of air
ρ_f	Density of fuel
v_f	Fuel kinematic viscosity